PVP-mediated galvanic replacement growth of AgNPs on copper foil for SERS sensing

Hui Xiang Wu[1], *Ming Cong Rong*[1], *Yi Ma*[2] ✉, *Shan Duo Chen*[3]

[1]*School of Chemistry and Chemical Engineering/Guangzhou Key Laboratory for Clean Energy and Materials, Guangzhou University, Guangzhou 510006, People's Republic of China*
[2]*College of Bioengineering, Sichuan University of Science and Technology, Zigong 643000, People's Republic of China*
[3]*College of Life Science, Guangzhou University, Guangzhou 510006, People's Republic of China*
✉ *E-mail: zhangyer2008@suse.edu.cn*

Published in Micro & Nano Letters; Received on 6th March 2020; Revised on 8th April 2020; Accepted on 20th April 2020

Herein, the authors present a simple and cost-effective silver nanoparticles (AgNPs)-based surface-enhanced Raman scattering (SERS) sensor based on galvanic displacement reaction using $AgNO_3$ and copper foil as precursors. With the mediation of polyvinyl pyrrolidone (PVP), AgNPs grow in-situ on the surface of copper foil at room temperature. AgNPs-based SERS sensor was prepared with optimised $AgNO_3$ concentration of 50 mM, the mass ratio of $AgNO_3$ to PVP of 2:1 and characterised using scanning electron microscopy and X-ray diffraction. As-fabricated SERS sensor exhibited a high Raman signal enhancement factor of 3.5×10^5 in the detection of Rhodamine 6G (R6G). Furthermore, a decent linear relationship for methyl parathion sensing was obtained in the range from 1×10^{-6} to 1×10^{-4} M, with an actual detection limit of 1×10^{-6} M. Recoveries of methyl parathion-spiked lake water samples ranging from 93.64 to 106.16% were obtained, suggesting the feasibility of the SERS sensor. These features demonstrated that the AgNPs-based SERS sensor can potentially be used in sensing a trace amount of chemicals in surface water for environmental protection.

1. Introduction: Surface-enhanced Raman scattering (SERS) derives from tremendous electromagnetic enhancement of noble nanostructured materials (Au, Ag etc.) in the excited photoelectric field, which enables a sharp increase in Raman signals of organic molecules near the nanostructured region [1–3]. In addition, the specific finger-prints (SERS spectra) of the given molecules offer it an excellent anti-disturbance capacity towards the analytes of interests [4]. Thus, an increasing amount of interests are dedicated to the development of organic molecules sensors using SERS effect since its discovery in 1974 [5–7]. For SERS sensors, it is of paramount significance for the fabrication of SERS substrate in effective detection of targets. In the past, there were intensive reports on the preparation of colloidal noble nanoparticles (CNNPs) with various shapes and sizes for the SERS detection of targets in solutions [3, 8]. Many SERS 'hot spots' can be formed by the assembly of CNNPs, further giving it good sensitivity. In spite of success above, difficulty in achieving uniform CNNPs and 'hot spots' are still detrimental to the applications of SERS sensors. Therefore, it remains necessary to exploit a solid-SERS sensor for their real applications.

In order to fabricate large-scale and highly controllable SERS substrates, a host of strategies have been utilised, such as electron beam lithography [9], ion beam lithography [10], physical vapor deposition [11], nanoimprint lithography [12] and so on. However, either time-consuming, high-cost or complex operating procedures of these techniques hinder their widespread use [13]. Galvanic displacement reaction (GDR) has been proven to be a feasible mean to grow noble nanostructured materials on the appropriate substrates in a simple and highly efficient way [14–16]. For instance, some kinds of Ag nanostructured SERS substrates were fabricated using Al/Cu and $AgNO_3$ as precursors due to the high reactivity of the Ag^+/Al or Ag^+/Cu pairs [14, 16]. Albert *et al.* constructed an Ag dendrites-based SERS substrate via GDR on commercial aluminium foil [14], in which the Ag dendrites was formed all over the aluminium foil by immersing aluminium foil in the AgF solution for 24 h. Similarly, another strategy employed to development of Ag-nanostructured SERS substrate reported by Goodacre was by direct dropping $AgNO_3$ aqueous onto copper foil and incubation for a specified time, in which the effects of deposition time and incubation temperature on the morphologies of SERS Ag-nanostructured substrate were investigated [15]. Although easiness of operation and cost-effectiveness can be achieved using the above protocols, reproducibility of SERS is still unsatisfactory owing to the uncontrollable growth of Ag-nanostructured material.

A number of studies show that polyvinyl pyrrolidone (PVP) is an effective capping reagent for regulating the growth of Ag nanomaterial [17–19]. PVP can selectively bind to (100) facet of Ag to slow down their growth rate, leading to the formation of silver nanoparticles (AgNPs) rather than Ag dendrites [17]. In this study, we were motivated to improve the design of the Ag-nanostructured SERS sensing platform on the copper foil using PVP as template agents to regulate the morphology of Ag. The effects of concentrations of $AgNO_3$ and the mass ratio of $AgNO_3$ to PVP were systematically investigated and consequently AgNPs-based copper foil SERS sensor was obtained. Methyl parathion, a commonly used organophosphorus pesticide, was selected as a model Raman probe to investigate the feasibility of as-presented SERS sensor. Good sensitivity and quantitative detection capacity for methyl parathion in aqueous solutions and favourable recoveries in lake water samples were acquired. These results demonstrate that as-fabricated SERS sensor can be a promising candidate for the detection of organic hazardous chemicals in real applications.

2. Experimental section

2.1. Materials and chemicals: Silver nitrate ($AgNO_3$) (≥99.9%), methyl parathion, PVP (MW ¼ 1300000) and Rhodamine 6G (R6G) were obtained from Sigma-Aldrich. Copper foil was bought from Minnesota Mining and Manufacturing Company. Methyl parathion and R6G were of analytical purity. The deionised water was generated using water purification system (Milli-Q Academic A10, Millipore).

2.2. Instrument and apparatus: The scanning electron microscopy (SEM) images were taken by a field emission scanning electron microscope (JEOL 6335F, Thermo Fisher Scientific Ltd.). X-ray diffraction (XRD) patterns were recorded by a Rigaku Ultima IV diffractometer. A portable Raman spectrometer (QE Pro, Ocean Optics) coupled with a 785 nm laser was used to collect the Raman spectra. During the detection, the integration time of the Raman spectra was 5 s.

doi: 10.1049/mnl.2020.0148

2.3. Preparation of stock solutions: $AgNO_3$ (100 mM) and PVP (16.9 g/l) stock aqueous solutions were obtained by dissolving them into 40 ml deionised water, respectively. Mixture solutions of $AgNO_3$ and PVP with different mass ratio were prepared by mixing 1 ml of $AgNO_3$ stock solutions with various volume of PVP stock solutions, and finally the volumes were fixed to 2 ml using deionised water. The methyl parathion ethanol solution (stock solution) and R6G aqueous solutions with a concentration of 0.01 M were prepared by diluting 0.026 g methyl parathion into 10 ml absolute ethanol and 10 ml deionised water, respectively. Methyl parathion solutions of various concentrations were produced by diluting the stock solution by deionised water. To detect methyl parathion in lake water, lake water was firstly filtered with filter paper to remove large solid particles and spiked with methyl parathion of various concentrations.

2.4. Fabrication of SERS sensor and SERS measurement procedure: Copper foil tape was cut into small slices (0.5 cm × 0.5 cm) and paste them onto the glass substrate. Then the copper slices were washed using ultrasonic machine for 30 s, followed by rinsed with absolute ethanol and deionised water successively to remove the impurities. For preparing the Ag dendrites, 3 µl $AgNO_3$ aqueous solutions with various concentrations (10, 50, 100 mM) were dropped onto the centre of copper slices and dried at room temperature. Similarly, 3 µl of freshly prepared mixture solutions of $AgNO_3$ and PVP solutions with various mass ratios (1:1, 2:1, 4:1, 6:1) were dropped onto the centre of copper slices and leaving for drying at room temperature to acquire AgNPs. Afterwards, 2 µl of sample solutions (methyl parathion, R6G) was dropped onto the SERS substrate and SERS spectra were recorded immediately using a portable Raman spectrometer. Each single SERS spectrum was collected using one freshly prepared SERS substrate using the above-mentioned procedures.

3. Results and discussion

3.1. Characterisation of SERS substrate: The effect of $AgNO_3$ concentrations without the addition of PVP was first investigated and the morphologies of Ag nanostructured materials were shown in Fig. 1.

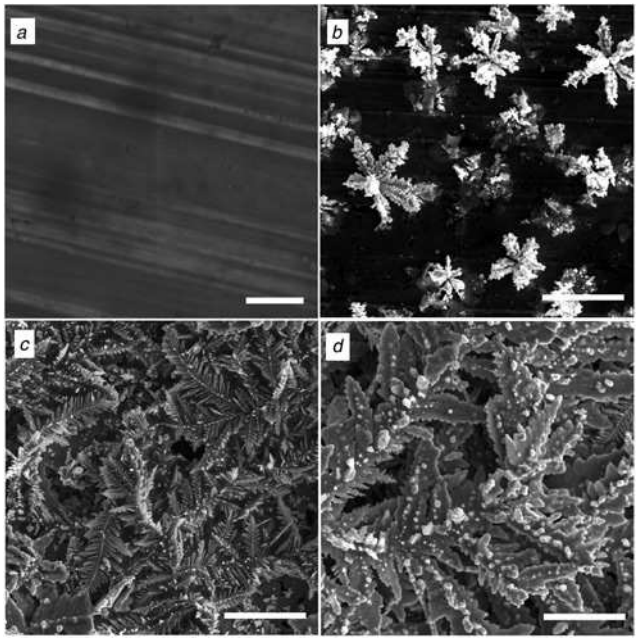

Fig. 1 *SEM images of*
a Copper foil
b–d Silver nanostructure grown on copper foil with different concentrations of $AgNO_3$ (*b–d*: $AgNO_3$ concentrations are 10, 50 and 100 mM, respectively; scale bar is 6 µm)

Fig. 1*a* shows the surface morphology of copper foil. Some wispy stripes were observed, which may be resulted from scrape during the cutting and washing the copper foil. Upon addition of 10 mM of $AgNO_3$, the replacement reaction ($Cu + 2Ag^+ = Cu^{2+} + 2Ag$) happened. Due to the high reactivity of the Ag^+/Cu, some Ag seeds were formed on the surface of Cu foil randomly and grew to amorphous Ag rapidly and some grass-like Ag nanoclusters (Fig. 1*b*) were sporadically distributed on the surface of copper foil and many nanogaps (hot spots) (Fig. 2*a*) can be acquired within a single cluster. However, insufficient coverage resulted from low $AgNO_3$ concentrations is a disadvantage for the SERS detection of targets. High $AgNO_3$ concentrations are in favour of increasing the nucleation rate of Ag clusters according to the proposed original nucleation-growth mechanism [20]. As such, addition of 50 mM of $AgNO_3$ can provide more growth points and Ag dendrites were acquired, being beneficial for the increase of coverage (Fig. 1*c*). Furthermore, Fig. 2*b* shows that the Ag dendrites own relatively flat morphology and many needle-like nanostructures, which was supposed to be good for the effective SERS detection of analytes. In contrast, when we increased the $AgNO_3$ concentration to 100 mM, as shown in Fig. 1*d* and Fig. 2*c*, hypermorphosis of Ag nanomaterials leads to their relatively low homogeneity and loss of fine structures. Thus, $AgNO_3$ concentration of 50 mM was selected as an appropriate one for further study.

Owing to the high reactivity of the Ag^+/Cu pair, nucleation and growth of Ag is in relatively bad controllability. In this case, a series of PVP solutions were mixed with 50 mM $AgNO_3$ (mass ratios of $AgNO_3$ to PVP were 1:1, 2:1, 4:1, 6:1) to control the morphologies of Ag nanostructured materials. The PVP used as a capping agent is able to selectively bind to the (100) facets of Ag nanocrystals, favouring the formation of nanoparticles [17]. As shown in Fig. 3*a*, anomalous AgNPs were obtained after addition of equivalent PVP. Excessive loading of PVP accumulated onto the surface of AgNPs, being a disadvantage for SERS detection of targets. As a reduction of the addition of PVP ($AgNO_3$: PVP of 2:1), AgNPs with a good mono-dispersity were obtained and excessive PVP were disappeared (Fig. 3*b*). Obviously, with a further reduction of the addition of PVP, the agglomeration degree of AgNPs clusters increases gradually, which is detrimental for effective SERS detection. Therefore, the mass ratio of $AgNO_3$ to PVP of 2:1 can be an optimal additive amount of PVP.

In order to investigate the phase and chemical structure of as-prepared Ag nanostructured SERS sensors, XRD characterisation was performed. As shown in Fig. 4*a*, XRD spectrum (black) of copper foil displays three diffraction peaks at 2θ of 43.6°, 50.7° and 74.3°, corresponding to its (111), (200) and (220) lattice planes (JCPDS04-0836 (Cu)). For Ag dendrites (red) and AgNPs (blue), four new discernable peaks at 2θ of 38.2°, 44.3°, 64.3° and 74.4° appeared, which corresponds to (110), (200), (220) and (311) lattice planes of Ag [21]. The faint peaks at 50.7° and 74.3° of AgNPs can be ascribed to the existence of PVP, which obstructed the penetration of X-ray. In addition, the rise of three peaks at 36.5°, 42.4° and 61.4° can be ascribed to the oxides of Ag (JCPDS40-1054 (Ag_3O_4)). In addition, the typically selected area of energy dispersive X-ray spectroscopy (EDX) spectrum of the AgNPs-based SERS substrate (Fig. 4*b*) verifies

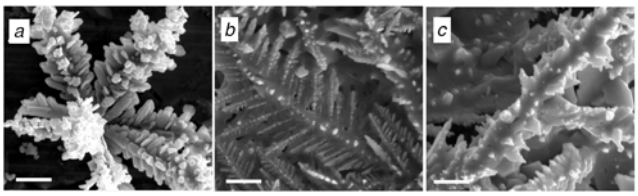

Fig. 2 *SEM images of silver nanostructure grown on copper foil with different concentration of $AgNO_3$*
a–c $AgNO_3$ concentrations are 10, 50 and 100 mM, respectively; scale bar is 1 µm

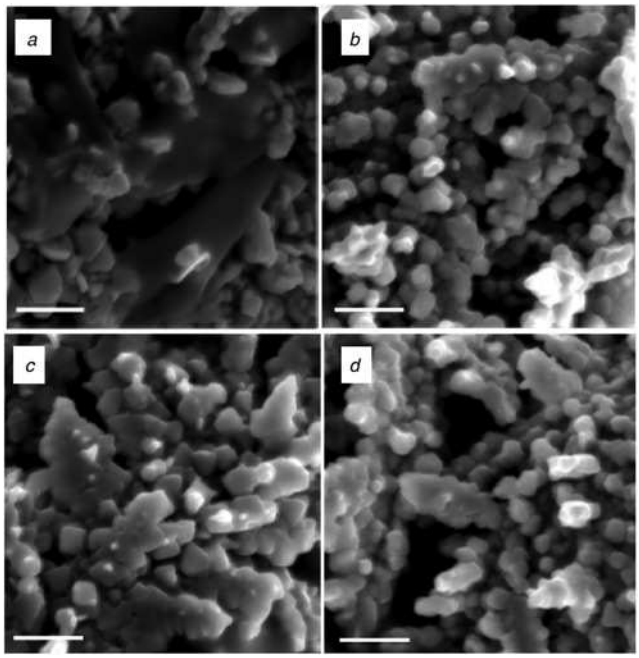

Fig. 3 *SEM images of Ag nanostructure with the addition of various amount of PVP*
a–d Weight ratio of $AgNO_3$ to PVP are 1:1, 2:1, 4:1, 6:1, respectively; scale bar is 1 μm

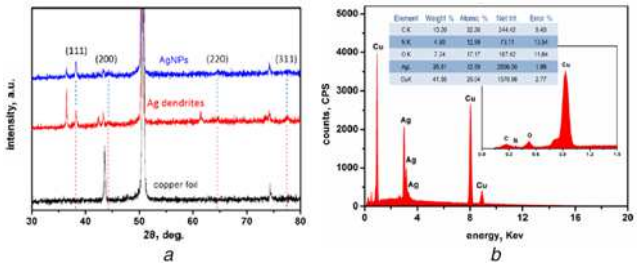

Fig. 4 *XRD and EDX patterns of Ag-nanostructure-based sensor*
a XRD patterns of copper foil, Ag dendrites and AgNPs
b EDX spectrum of AgNPs-based SERS substrate

the presence of Ag, Cu, C, O, N, and these elements are homogenously distributed throughout the whole SERS substrate. These observations further confirmed the successful preparations of Ag nanostructured SERS sensors.

3.2. Analytical performances of as-prepared SERS sensors: Afterwards, we first conducted the SERS test for methyl parathion using Ag dendrites and the SERS spectra of Raman shift from 700 to 1430 cm^{-1} were recorded. As shown in Fig. 5*a*, no evident peak was observed for Ag dendrites, suggesting a low background interference of the SERS substrate. After addition of 1×10^{-6} M of methyl parathion, a scatter peak at 1347 cm^{-1} assigned to C–H bend stretch was observed. At higher concentrations of methyl parathion, two more peaks at 858 and 1117 cm^{-1} appeared, which can be attributed to the P–O and C–N stretch, respectively. The assignments of these peaks were listed in Table 1, which reaches a great agreement with previous reports [22, 23]. However, some baselines drifted obviously. We further confirmed the reproducibility of the sensor. We prepared 20 SERS substrates to detect the 1×10^{-5} M of methyl parathion and collected the intensities of peaks at 1347 cm^{-1}. As displayed in Fig. 5*b*, the relative standard deviation (RSD) of the assay was 31.92%, which can be attributed to a lot of large cavities of Ag dendrites. It indicates a poor reproducibility and precision of the sensor.

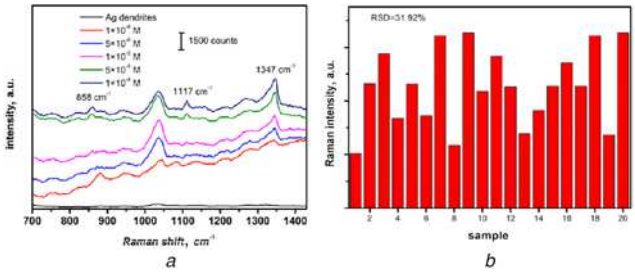

Fig. 5 *Analytical performances of Ag-dendrites-based sensor on methyl parathion*
a SERS detection of methyl parathion with various concentrations on Ag dendrites
b Reproducibility of Ag dendrites SERS substrate on methyl parathion

Table 1 Assignments of SERS peaks for R6G and methyl parathion

Chemicals	Raman shift, cm^{-1}	Assignment
Rodamine 6G (R6G)	608	in-plane bend of the xanthene core
	769	phenyl ring
	1123	phenyl ring, xanthene core and amide group
	1194	xanthene core and amide group
	1311	xanthene core and amide group
	1361	xanthene core and amide group
	1509	xanthene core and amide group
	1647	xanthene core
Methyl parathion	1111/1117	stretching vibration of C–N
	858	stretching vibration of P–O
	1347	bending vibration of C–H

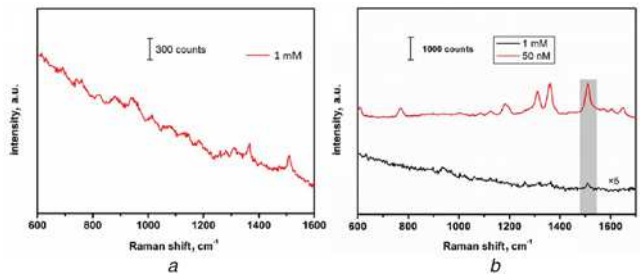

Fig. 6 *Raman spectra of R6G for enhancement factor calculation*
a Raman spectrum of R6G on Cu foil
b Raman spectrum of R6G on silicon wafer and R6G recorded on AgNPs-based SERS sensors

The analytical performances of the AgNPs-based SERS sensor were also studied. The SERS enhancement factor (EF) of the sensor was first studied using R6G as model Raman dye. Fig. 6 and Table 2 show the Raman spectrum of R6G and corresponding Raman intensities with a concentration of 1×10^{-3} M on Cu foil and silicon wafer (5 times), as well as SERS spectrum of R6G with a concentration of 5×10^{-8} M. Raman spectra of high concentration (1×10^{-3}) R6G shows three relatively weak peaks at 1311, 1361 and 1509 cm^{-1}. By contrast, SERS spectrum of R6G with much lower concentration was collected on the sensor, besides three aforementioned peaks, another five distinct peaks appeared at 608, 769, 1123, 1194 and 1647 cm^{-1}, accompanied with a significantly enhanced Raman signal (all these molecule vibration assignments were listed in Table 1 [21, 24]). The relatively low Raman intensity of R6G on Cu foil (high concentration) compared to that of SERS spectrum on AuNPs-based SERS substrate (much lower concentration) indicates a little background interference of Cu foil on the detection of analytes. The EF of the sensor was determined

doi: 10.1049/mnl.2020.0148

Table 2 Values of measured I_{SERS} on SERS sensors, I_{NRS} on silicon wafer and Cu foil; value of C_{SERS} and C_{NRS} as well as the calculated EFs

Substrate	I_{SERS} (counts)	I_{NRS} (counts)	C_{SERS} (M)	C_{NRS} (M)	EF
Cu foil	—	312	—	1×10^{-3}	—
SERS sensor	1187	68	5×10^{-8}	1×10^{-3}	3.5×10^{5}

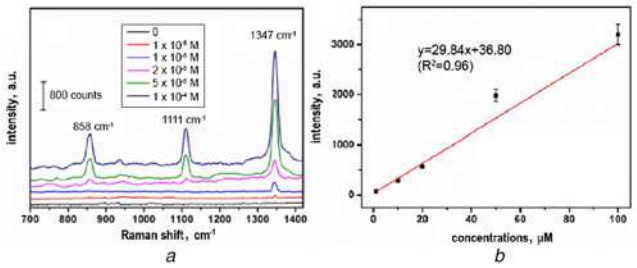

Fig. 7 *Quantitative analysis of methyl parathion on AgNPs-based sensor*
a Raman spectra of different concentrations of methyl parathion residues detected on Ag nanoparticles grown on copper foil
b Corresponding calibration curve of Raman intensity versus the surface concentrations of methyl parathion

using the reported equation [25]

$$\mathrm{EF} = \frac{I_{SERS}/C_{SERS}}{I_{NRS}/C_{NRS}}$$

where I_{SERS} and I_{NRS} are the integrated SERS and normal Raman scattering (NRS) intensities of R6G at the same band, respectively. C_{SERS} and C_{NRS} are the concentrations of probed molecules in the SERS and NRS measurements, respectively. Raman and SERS intensities with baseline correction of R6G at 1509 cm^{-1} were extracted (Table 2) for EF calculation and EF value of 3.5×10^5 was acquired.

Fig. 7*a* shows the Raman spectra of methyl parathion recorded from 700 to 1430 cm^{-1} on the SERS sensor. There was no obvious scattering peak on pure SERS substrate, implying no background interference. Upon addition of 1×10^{-6} M of methyl parathion, scattering peak at 1347 cm^{-1} appeared. Two more peaks at 858 cm^{-1} and 1111 cm^{-1} occurred after addition of concentrations of 2×10^{-5} M. In addition, the Raman intensities increased gradually with the increasing concentrations of methyl parathion. Fig. 7*b* shows a fine linear relationship ($R^2 = 0.96$) between Raman intensities at 1347 cm^{-1} of methyl parathion with concentrations ranging from 1×10^{-6} to 1×10^{-4} M, with an actual detection limit of 1×10^{-6} M ($n = 5$). Furthermore, the reproducibility of the sensor was testified. A much better reproducibility was obtained compared to Ag dendrites-based sensor. Twenty methyl parathion samples with the concentration of 1×10^{-5} M were tested and the RSD of assays obtained was 10.27% (Fig. 8).

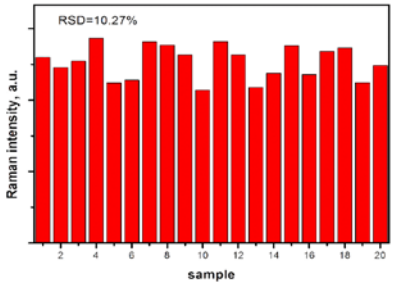

Fig. 8 *Reproducibility of AgNPs SERS substrate on methyl parathion*

Table 3 Recoveries test of methyl parathion spiked lake water samples

Samples	Added amount, μM	Detected amount, μM	RSD, %	Recoveries, %
1	10	9.36	10.47	93.64
2	50	53.08	11.53	106.16
3	100	101.58	9.38	101.58

To study the potential real application of the developed AgNPs-based SERS sensing platform, detection of methyl parathion spiked lake water samples with desired analyte concentrations were performed. The Raman peak intensities at 1347 cm^{-1} were used to calculate the recovery ($n = 5$). As shown in Table 3, recoveries of methyl parathion in spiked lake water ranged from 93.64 to 106.16% with a RSD <11.53%, suggesting favourable recoveries for methyl parathion detection in lake water samples. These results have demonstrated that the AgNPs-based SERS sensing strategy holds great potential in real applications for environment protection.

4. Conclusion: In summary, a simple and cost-effective AgNPs-based SERS sensor was fabricated by using GDR between $AgNO_3$ and copper foil mediated by PVP. A wide linear range and low detection obtained from testing of methyl parathion aqueous samples demonstrated a good analytical performance of as-fabricated SERS sensor. In addition, the feasibility of the sensor was verified by methyl parathion spiked lake water samples detection. All these features suggested that the AgNPs-based SERS sensor can potentially be used in sensing a trace amount of chemicals for environmental protection.

5. Acknowledgments: This work was supported by National Natural Science Foundation of China (31801458), Talent introduction program of Sichuan University of Science and Engineering (2017RCL24), Guangdong Natural Science Foundation (2017A030310652, 2019A1515011328), Featured Innovation Project of Guangdong Province Office of Education (2018KTSCX180) and Science and Technology Research Project of Guangzhou (201804010117)

6 References

[1] Mosier-Boss P.A.: 'Review of SERS substrates for chemical sensing', *Nanomaterials*, 2017, **7**, (6), p. 142
[2] Pang S., Yang T., He L.: 'Review of surface enhanced Raman spectroscopic (SERS) detection of synthetic chemical pesticides', *Trac-Trends Anal. Chem.*, 2016, **85**, (SI), pp. 73–82
[3] Wu H., Luo Y., Huang Y., *ET AL.*: 'A simple SERS-based trace sensing platform enabled by AuNPs-analyte/AuNPs double-decker structure on wax-coated hydrophobic surface', *Front. Chem.*, 2018, **6**, p. 482
[4] Wang Y., Yan B., Chen L.: 'SERS tags: novel optical nanoprobes for bioanalysis', *Chem. Rev.*, 2013, **113**, (3), pp. 1391–1428
[5] Fleischmann M., Hendra P.J., Mcquillan A.J.: 'Raman spectra of pyridine adsorbed at a silver electrode', *Chem. Phys. Lett.*, 1974, **26**, (2), pp. 163–166
[6] Jeanmaire D.L., Duyne R.P.V.: 'Surface Raman spectroelectrochemistry: part I. Heterocyclic, aromatic, and aliphatic amines adsorbed on the anodized silver electrode', *J. Electroanal. Chem. Interfacial Electrochem.*, 1977, **84**, (1), pp. 1–20
[7] McNay G., Eustace D., Smith W.E., *ET AL.*: 'Surface-enhanced Raman scattering (SERS) and surface-enhanced resonance Raman scattering (SERRS): a review of applications', *Appl. Spectrosc.*, 2011, **65**, (8), pp. 825–837
[8] Peng B., Li G., Li D., *ET AL.*: 'Vertically aligned gold nanorod monolayer on arbitrary substrates: self-assembly and femtomolar detection of food contaminants', *ACS Nano*, 2013, **7**, (7), pp. 5993–6000
[9] Chirumamilla M., Toma A., Gopalakrishnan A., *ET AL.*: '3D nanostar dimers with a sub-10-nm gap for single-/few- molecule surface-enhanced Raman scattering', *Adv. Mater.*, 2014, **26**, (15), pp. 2353–2358

[10] Cialla D., Hubner U., Schneidewind H., *ET AL.*: 'Probing innovative microfabricated substrates for their reproducible SERS activity', *ChemPhysChem*, 2008, **9**, (5), pp. 758–762
[11] Sun X., Stagon S., Huang H., *ET AL.*: 'Functionalized aligned silver nanorod arrays for glucose sensing through surface enhanced Raman scattering', *RSC Adv.*, 2014, **4**, (45), pp. 23382–23388
[12] Yao J, Le A.P., Gray S.K., *ET AL.*: 'Functional nanostructured plasmonic materials', *Adv. Mater.*, 2010, **22**, (10), pp. 1102–1110
[13] Xie X., Pu H., Sun D.W.: 'Recent advances in nanofabrication techniques for SERS substrates and their applications in food safety analysis', *Crit. Rev. Food Sci.*, 2017, **58**, (16), pp. 1–14
[14] Gutes A., Carraro C., Maboudian R.: 'Silver dendrites from galvanic displacement on commercial aluminum foil as an effective SERS substrate', *J. Am. Chem. Soc.*, 2010, **132**, (5), pp. 1476–1477
[15] Mabbott S., Larmour I.A., Vishnyakov V., *ET AL.*: 'The optimisation of facile substrates for surface enhanced Raman scattering through galvanic replacement of silver onto copper', *Analyst*, 2012, **137**, (12), pp. 2791–2798
[16] Guo T.L, Li J.G, Sun X., *ET AL.*: 'Improved galvanic replacement growth of Ag microstructures on Cu micro-grid for enhanced SERS detection of organic molecules', *Mater. Sci. Eng. C-Mater.*, 2016, **61**, pp. 97–104
[17] Zhang Q., Li W., Wen L.P., *ET AL.*: 'Facile synthesis of Ag nanocubes of 30 to 70 nm in edge length with CF_3COOAg as a precursor', *Chem-Eur. J.*, 2010, **16**, (33), pp. 10234–10239
[18] Sun Y., Mayers B., Herricks T., *ET AL.*: 'Polyol synthesis of uniform silver nanowires A plausible growth mechanism and the supporting evidence'. *Nano Lett.*, 2003, **3**, (7), pp. 955–960
[19] Wiley B.J., Chen Y., McLellan J.M., *ET AL.*: 'Synthesis and optical properties of silver nanobars and nanorice', *Nano Lett.*, 2007, **7**, (4), pp. 1032–1036
[20] Ji X., Song X., Li J., *ET AL.*: 'Size control of gold nanocrystals in citrate reduction: the third role of citrate', *J. Am. Chem. Soc.*, 2007, **129**, (45), pp. 13939–13948
[21] Wu H., Sun X., Hou C., *ET AL.*: 'Preparation of quasi-three-dimensional porous Ag and Ag-Nio nanofibrous mats for SERS application', *Sensors*, 2018, **18**, (9), p. 2862
[22] Wu H., Luo Y., Hou C., *ET AL.*: 'Flexible bipyramid-AuNPs based SERS tape sensing strategy for detecting methyl parathion on vegetable and fruit surface', *Sens. Actuat. B, Chem.*, 2019, **285**, pp. 123–128
[23] Lee D., Lee S., Seong G.H., *ET AL.*: 'Quantitative analysis of methyl parathion pesticides in a polydimethylsiloxane microfluidic channel using confocal surface-enhanced Raman spectroscopy', *Appl. Spectrosc.*, 2006, **60**, (4), pp. 373–377
[24] Shim S., Stuart C.M., Mathies R.A.: 'Resonance Raman cross-sections and vibronic analysis of rhodamine 6G from broadband stimulated Raman spectroscopy', *ChemPhysChem*, 2008, **9**, (5), pp. 697–699
[25] Wustholz K.L., Henry A.I., McMahon J.M., *ET AL.*: 'Structure-activity relationships in gold nanoparticle dimers and trimers for surface-enhanced Raman spectroscopy', *J. Am. Chem. Soc.*, 2010, **132**, (31), pp. 10903–10910

doi: 10.1049/mnl.2020.0148